Geophysical Research Letters

RESEARCH LETTER
10.1029/2021GL095362

A Climatology of Narrow Cold-Frontal Rainbands in Southern California

Marian de Orla-Barile[1], Forest Cannon[1], Nina S. Oakley[1], and F. Martin Ralph[1]

[1]Center for Western Weather and Water Extremes – Scripps Institution of Oceanography, University of California, San Diego, CA, USA

Key Points:

- Southern California experienced 94 narrow cold-frontal rainbands over 26 water years from 1995 to 2020
- Common synoptic conditions associated with narrow cold-frontal rainband development include a deepening cyclone off of the California coast
- Future work can focus on the development of automated detection algorithms for NCFR identification using radar, and improved forecasting

Supporting Information:

Supporting Information may be found in the online version of this article.

Correspondence to:

M. de Orla-Barile,
mariandeorla-barile@ucsb.edu

Citation:

de Orla-Barile, M., Cannon, F., Oakley, N. S., & Ralph, F. M. (2022). A climatology of narrow cold-frontal rainbands in Southern California. *Geophysical Research Letters*, *49*, e2021GL095362. https://doi.org/10.1029/2021GL095362

Received 22 JUL 2021
Accepted 9 DEC 2021

Author Contributions:

Conceptualization: Marian de Orla-Barile, Forest Cannon
Formal analysis: Marian de Orla-Barile, Forest Cannon
Funding acquisition: F. Martin Ralph
Investigation: Marian de Orla-Barile, Nina S. Oakley
Methodology: Marian de Orla-Barile, Forest Cannon, Nina S. Oakley
Resources: Nina S. Oakley, F. Martin Ralph
Supervision: Forest Cannon, Nina S. Oakley, F. Martin Ralph
Visualization: Marian de Orla-Barile

Abstract Narrow cold-frontal rainbands (NCFRs) produce short-duration, high-intensity precipitation associated with flash flooding and debris flows in Southern California, including the extremely destructive 2018 Montecito event. This manuscript presents the first known catalog of NCFR events in this region during winter seasons 1995–2020. A manual approach was used to identify NCFRs in radar imagery, supported by rain gauges and atmospheric reanalysis products. In total, 94 NCFRs were observed, with an average of three landfalling events occurring per water year. Propagation and impacts of these NCFRs were also investigated. Composite analyses of synoptic conditions reveal similarities across events; however, individual NCFRs exist on a spectrum of atmospheric conditions, precipitation intensity, and associated hazards. This regional record serves as a control dataset for the development of an objective identification algorithm and supports the evaluation and improvement of forecasting procedures. Methods established here are transferrable to other mid-latitude regions with limited radar coverage.

Plain Language Summary Narrow cold-frontal rainbands produce short-duration (<1-hr), high-intensity precipitation associated with flash floods and debris flows in Southern California, including the extremely destructive 2018 Montecito event. Prior research describes development, predictability, and associated hazards of these bands, though no known long-term record of their occurrence and climatological characteristics exists within the United States. This study provides the first known catalog of narrow cold-frontal rainbands during the winter seasons of 1995–2020 in Southern California, and explores characteristics of these features such as frequency, movement, and the large-scale meteorology that drives them. Events were documented manually using rain gauge observations, radar data, and output from atmospheric models. In total, 94 rainbands were documented during the study period, with an average of three landfalling events occurring in Southern California per water year. The intensity and impacts across the recorded events varied, though common weather patterns, including strengthening cyclones near the California coast, were associated with the documented events. This catalog supports weather forecasting efforts as well as the future development of an automated detection algorithm.

1. Introduction

Narrow cold-frontal rainbands (NCFRs) generate short-duration, high-intensity precipitation with notable impacts in Southern California (Cannon et al., 2018; Oakley et al., 2017; Sukup et al., 2016), which include the destructive and deadly 2018 Montecito debris flow (County of Santa Barbara, 2018; Lukashov et al., 2019; Oakley, Cannon, Munroe, et al., 2018). Existing research provides a comprehensive understanding of the meteorological characteristics of NCFRs using observations and models (e.g., Carbone, 1982; Geerts & Hobbs, 1995; Houze et al., 1976; Jorgensen et al., 2003; Parsons, 1992). Recent case studies have documented NCFR occurrence, characteristics, and predictability in several events that impacted Southern California (e.g., Cannon et al., 2018, 2020; Oakley, Cannon, Munroe, et al., 2018; Sukup et al., 2016). However, prior to this work, no known long-term record of NCFR occurrence in Southern California had been established. The primary objective of this study was to create a radar-based record of NCFRs in the Southern California Bight (hereafter "the Bight"), describe their climatological characteristics, frequency and impacts, and discuss future applications of the developed record.

Establishing a record of NCFRs in Southern California benefitted from past studies that developed manual, radar-based records of NCFRs as well as other convective lines in various regions (Clark, 2013; Clark & Parker, 2020; Gatzen, 2011; Trapp et al., 2005), and that generated automated methods to track mesoscale convective systems in other parts of the United States (e.g., Haberlie & Ashley, 2019; Prein et al., 2017). However, the

Writing – original draft: Marian de Orla-Barile, Forest Cannon
Writing – review & editing: Marian de Orla-Barile, Forest Cannon, Nina S. Oakley

application of automated methods in Southern California was not pursued due to region-specific radar limitations such as radar elevation and topographic blocking (Maddox et al., 2002; National Research Council, 2005; Thompson, 2001). These limitations are exacerbated by regional NCFR characteristics. Notably, the relatively shallow convective precipitation signal (typically <3 km in height; Hobbs & Biswas, 1979; Hobbs et al., 1978), gap and core structure (Cannon et al., 2020; Jorgensen et al., 2003), and topographic interactions (Neiman et al., 2004) collectively degrade the ability of the regional radar network to identify NCFRs.

This manuscript presents a manual approach to NCFR identification that leveraged both radar data and additional meteorological datasets to overcome the described radar limitations. These methods may be transferrable to other mid-latitude locations where radar is available and limited in coverage. In addition to cataloging NCFRs, synoptic conditions associated with events were evaluated in the context of several recent extreme events (Cannon et al., 2018, 2020; Oakley, Cannon, Munroe, et al., 2018). Further, National Weather Service (NWS) Watches, Warnings and Advisories (WWAs) were used to quantify typical hazards associated with NCFRs. The results presented address an immediate need in Southern California-specific meteorological research and operations, including subsequent research on objective methods for identifying and tracking NCFRs, quantifying regional radar limitations, and evaluating the representation of NCFRs in both nowcasting and numerical weather prediction.

2. Data and Methods

The NCFR identification process utilized a quality-controlled hourly precipitation dataset, gridded daily precipitation product, archived radar imagery, and an atmospheric reanalysis for the period October-May 1995–2019 and January–May for 2020 only. This period corresponds to the beginning of reliable and easily accessible archived radar imagery, as well the region's wet season, when extratropical cyclones bring the potential for NCFR development (Cannon et al., 2018). The ensuing descriptions outline each step taken in the NCFR identification process, which include using a 5 mm/hr threshold to identify precipitation events, subsequently viewing radar reflectivity imagery to search for narrow and long structures of at least 45 dBZ, and supporting identification decisions using reanalysis.

2.1. Precipitation Observations and Products

A record of moderate-to high-intensity precipitation dates was generated from 30 Remote Automatic Weather Station (RAWS; Zacharaissen et al., 2003) hourly tipping bucket rain gauges across Southern California (Figure 1). Precipitation data were quality controlled following the methods of Oakley, Lancaster, et al. (2018). A minimum hourly accumulation threshold of 5 mm was employed as a conservative baseline for identifying precipitation dates. This relatively low threshold, in addition to the vast majority of regional precipitation occurring in a handful of intense, short-duration winter storms each year (Lamjiri et al., 2018; Oakley, Cannon, Boldt, et al., 2018), mitigates the possibility of missing an event due to the gauge network's limited temporal and spatial sampling. In total, 4,349 individual hours exceeded the 5 mm threshold for at least one RAWS station and were subsequently evaluated in radar imagery (Section 2.1.3).

The Parameter Regression on Independent Slopes (PRISM; Daly et al., 1994) product was used as a supplemental method to ensure the RAWS analysis did not miss a potential event. The dates evaluated for NCFR activity (i.e., at least one 5 mm or greater observation at a minimum of one station) collectively accounted for between 85% and 95% of all PRISM precipitation at each individual pixel within the study domain (all grid cells in a box covering 32°–36°N, 122°–116°W). Thus, while the RAWS data set restricted our analyses to moderate intensity events, at a minimum, the relatively low threshold and buffer period that was employed resulted in a nearly complete record of Southern California precipitation.

2.2. Precipitation Radar

Level-II base reflectivity (https://www.ncdc.noaa.gov/wct/) and level-III composite reflectivity mosaics (https://www.ncei.noaa.gov/maps/radar/) from four regional NWS Next-Generation Weather Radar (NEXRAD; NOAA, 1991) installations were used to identify NCFRs. These included radars at San Diego (KNKX; 1996-present), Santa Ana (KSOX; 1997-present), Los Angeles (KVTX; 1995-present), and Vandenberg (KVBX; 1995-present, though a considerable amount of data was not archived for this site). Radar imagery concurrent

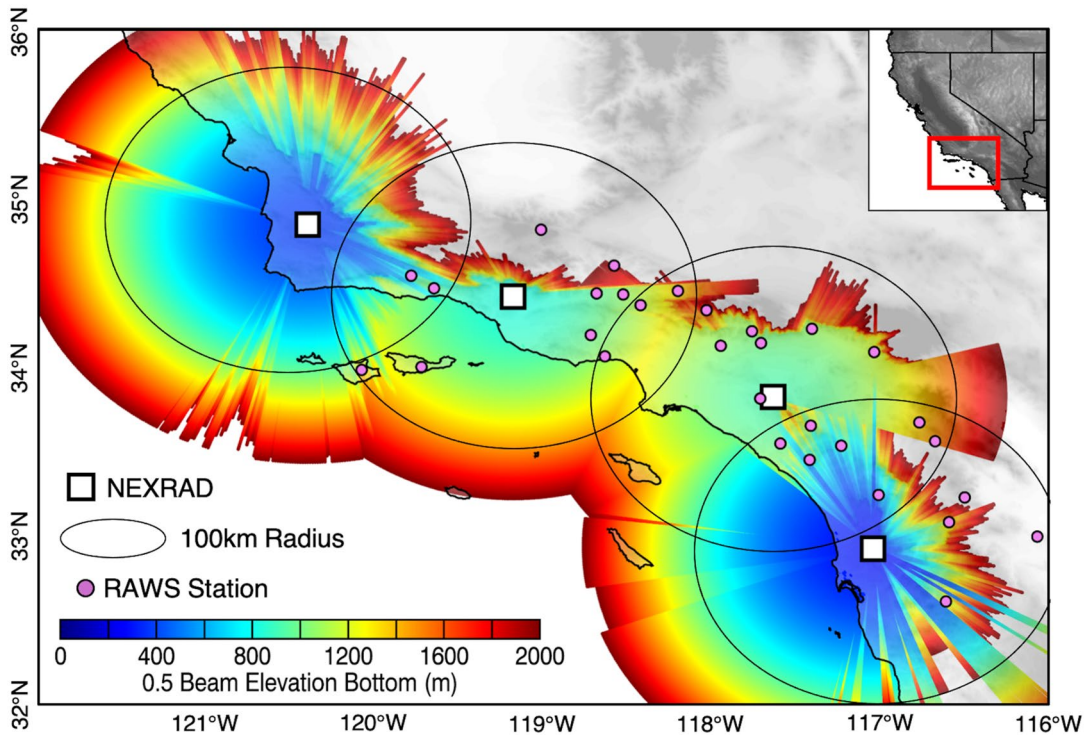

Figure 1. The minimum elevation of a 0.5° scan angle with a 1° beam width from each radar site as an approximation of minimum radar coverage height over the Bight (color fill; m). A radius of 100 km (black circles) is plotted for each radar (white squares). The location of the 30 RAWS stations (pink circles) used for NCFR identification are also shown.

with the gauge-based record of moderate-to-high intensity rainfall events was visually inspected at ~5 min intervals for evidence of narrow (e.g., visually appearing to be approximately several km in width), elongated (e.g., visually appearing to be approximately tens to hundreds of km in length), banded reflectivity structures exceeding 45 dBZ and propagating across the Bight. Length and width measurements were estimated visually, and were not quantified during analysis. The threshold of 45 dBZ was chosen based on previously studied narrow cold-frontal rainband events such as those found in Jorgensen et al. (2003; See their Section 3b and Figure 6), Oakley, Cannon, Munroe, et al. (2018; see their Figure 4), and Sukup et al. (2016; See their Figures 5, 7, and 8). During radar imagery inspection, the characteristic "gap and core" structure, which consists of high reflectivity cores and low reflectivity gap regions (e.g., Hobbs & Biswas, 1979; James & Browning, 1979; Jorgensen et al., 2003; Oakley, Cannon, Munroe, et al., 2018; Sukup et al., 2016), was also taken into consideration. In addition, radar imagery was typically viewed beyond the hourly intervals provided by the raingauge network if it was apparent that precipitation had been continuously occurring prior to or after any particular timestep.

While numerous radar tracking methods for convective features have been established in other locations (e.g., Haberlie & Ashley, 2019; Prein et al., 2017), a manual approach to NCFR identification—similar to that of Gatzen (2011)—was desirable to surmount the limitations of the regional radar network. As NCFRs are typically shallow convective features, their identification in radar is affected by elevation, range, beam broadening, and topographic blocking (e.g., Thompson, 2001). The four NEXRAD radar installations that cover the Bight range in elevation from ~300 to 1,000 m and have a base scan elevation angle of ~0.5°. Figure 1 demonstrates the minimum elevation of a 0.5° scan angle with a 1° beam width from each radar using a standard atmosphere and 4/3 Earth model (Doviak & Zrnić, 1993) to approximate minimum NEXRAD beam height over the Bight (color fill; m)—at just 100 km distance the majority of the radar beam is above 2 km altitude, which is higher than the NCFR signal extends in many cases (e.g., Cannon et al., 2020; Jorgensen et al., 2003). Because these limitations are event-dependent (e.g., the observed echo is affected by NCFR location, depth, intensity, interaction with topography in relation to radar scan geometry, and event freezing level height), developing a rules-based approach to automated detection would require a-priori knowledge of whether a NCFR had occurred.

2.3. Atmospheric Reanalysis

Hourly meteorological parameters (e.g., mean sea-level pressure, integrated water vapor, along with wind, temperature, geopotential heights, and specific humidity at 850 hPa, and winds at 250 hPa) from the European Center for Medium-Range Weather Forecasting fifth generation reanalysis (ERA5, 0.25° × 0.25° horizontal grid; Copernicus Climate Change Service, 2017) were used to identify synoptic characteristics of NCFR events and to evaluate variability across events in the catalog. The ERA5 reanalysis product also supported NCFR identification in questionable cases to determine if banded convective features were tied to a cold-front via examination of derived equivalent potential temperature (θ_e; Bolton, 1980).

2.4. National Weather Service Watches, Warnings, and Advisories

NWS WWAs were evaluated to quantify the relationship between NCFRs and regional hazard potential. The WWAs were obtained from the Iowa State University Iowa Environmental Mesonet archive (mesonet.agron.iastate.edu/request/gis/watchwarn.phtml) for the Los Angeles/Oxnard (LOX) and San Diego (SGX) NWS forecast offices responsible for forecasting over the Bight. Here, only "Warnings" in the "New" issuance category within 24 hr of the NCFR observations were considered to limit the analyses to high hazard-potential events. While NCFRs are often embedded within larger precipitating systems (e.g., atmospheric rivers—roughly two-thirds of the events were associated with an atmospheric river as identified by the methods of Rutz et al., 2014) the analyses were exclusive to warnings for flash floods, severe thunderstorms, and tornados, which can be associated with the extreme conditions generated by NCFRs (Oakley, Cannon, Munroe, et al., 2018; Sukup et al., 2016; Thompson, 2001), as opposed to atmospheric rivers. Proxy variables, such as streamflow or runoff, were not considered in this hazards analysis due to the complex nature of how they may relate to the spotty and fast moving precipitation associated with NCFRs.

2.5. Sensitivity Testing

The use of a manual, qualitative approach to identify NCFRs raises concern as to whether the climatology is complete and subsequent conclusions are accurate. Sensitivity testing to determine the impact of individual decisions was performed to ensure that the results presented here are robust and that any statements about NCFR climatology are insensitive to the inclusion or exclusion of a handful of individual events. Testing entailed both including and excluding questionable NCFRs from further analysis in addition to randomly sampling a subset of 50% of the NCFR events via Monte Carlo methods.

3. Results

3.1. Case Study: Narrow Cold-Frontal Rainband Example

The method to identify NCFRs in this study is best described through a representative example. A characteristic and impactful event that met the defined NCFR criteria occurred in Southern California on February 17–18, 2017. The meteorological conditions and regional impacts of this event are detailed in Cannon et al. (2018). The NCFR prompted issuances of multiple warnings by the NWS LOX and SGX Weather Forecast Offices, including flash flood warnings across the coastal Bight and adjacent mountains, and severe thunderstorm warnings for Orange and San Diego Counties.

From ∼23:00 to 04:00 UTC on February 17–18, 2017, multiple Southern California RAWS gauges reported hourly accumulations of ≥5 mm associated with the NCFR passage (Figure 2a). Radar imagery from 01:16 UTC on 18 February demonstrates a characteristic NCFR gap and core structure within the Bight, along with reflectivity values of ∼50–55 dBZ (Figure 2b). Over the subsequent hours the NCFR's northernmost cores near Los Angeles County weakened upon encountering coastal topography, while the southernmost cores intensified and impacted San Diego County at ∼02:30 UTC 18 February. Intensity and length/width requirements for identifying NCFRs defined in this study (Section 2.2) were met. The overall NCFR length was on the order of >400 km (though it likely extended beyond radar range to the south), and each of the cores was roughly 5–8 km in width and 25–50 km in length. The NCFR structure diminished by ∼04:00 UTC, giving way to broader scale and lighter precipitation as the associated atmospheric river propagated eastward over land.

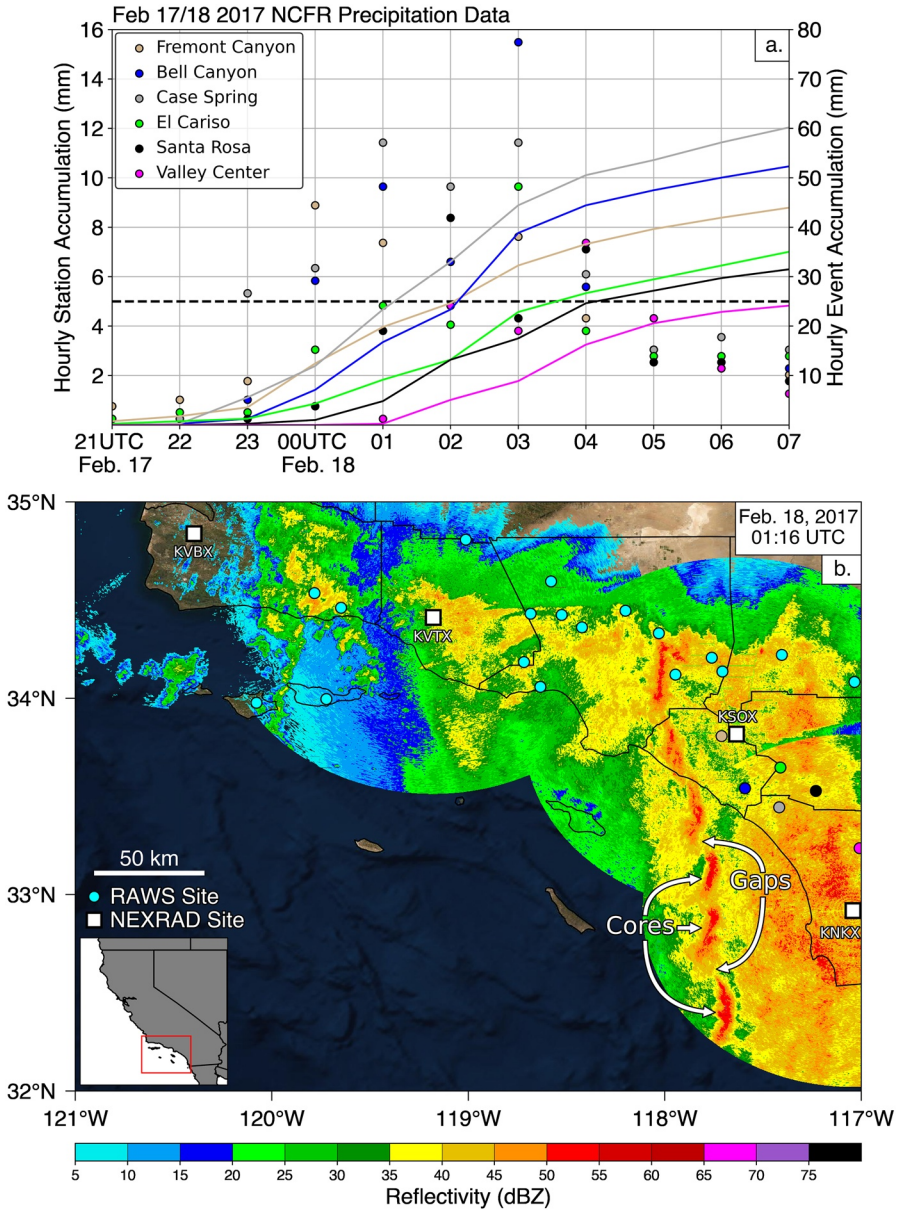

Figure 2. RAWS hourly accumulations during the passing of a NCFR in Southern California on February 17–18, 2017 (a). The black dotted line indicates the 5 mm hourly threshold. Radar reflectivity at 01:16 UTC on 18 February (b). The RAWS stations in (a) are colored accordingly in (b).

3.2. Record of NCFR Events

3.2.1. Seasonality

In the 26-year period considered in this study, 94 NCFRs were identified. In instances where multiple NCFRs were observed within the same 48-hr period, only the single maximum-intensity band was retained for synoptic weather and hazard impact analysis in order to not double count large-scale conditions (we term this an "NCFR episode," of which there are 76). On average, approximately three NCFRs occurred within the Bight per water year, with 6 of 26 water years actually experiencing three events (Figure S1 in Supporting information S1; note water year 1995 excludes the months of October–December 1994). The statistical range of NCFR events per water year was 10, demonstrating high interseason variability of passing NCFRs in the Bight. January, February, and March experienced the greatest number of NCFRs over the full record, with a total of 18, 20, and 18 in each

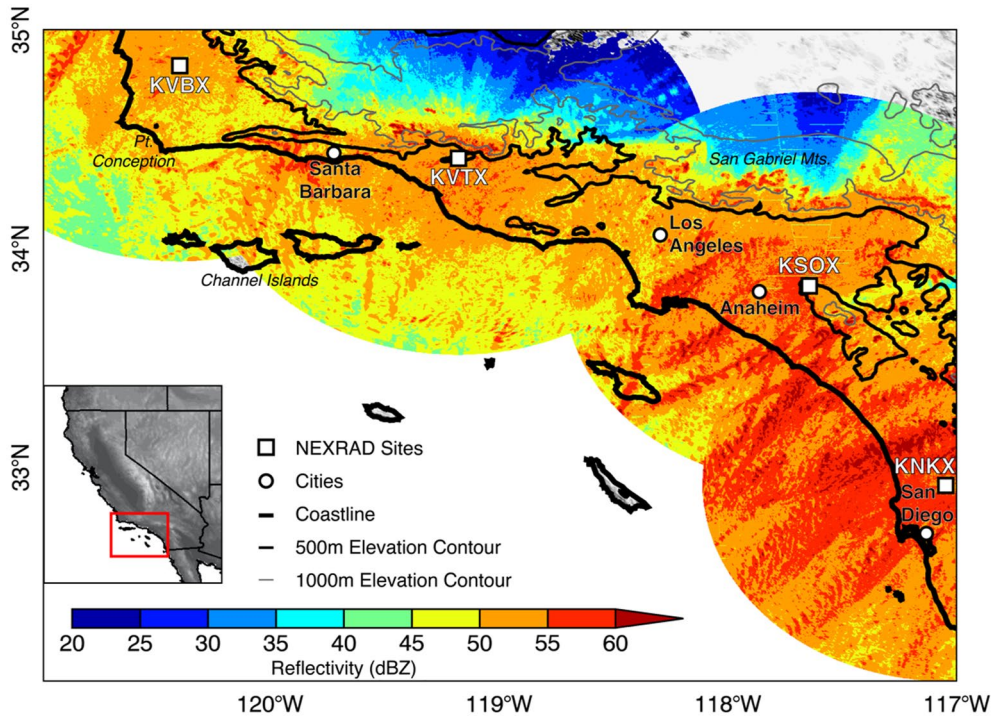

Figure 3. Maximum radar reflectivity within 100 km of four NEXRAD sites for 91 NCFRs (1996–2020) (color fill). Black contours identify topography at 500 m increments.

month respectively (Figure S2 in Supporting information S1). December experienced 16, November 10, April 6, October 3, and May 3 across the 26-year record (Figure S2 in Supporting information S1).

3.2.2. Reflectivity Characteristics

Maximum Level-II NEXRAD base reflectivity from each available regional radar for 91 NCFRs (all three NCFRs in 1995 did not have archived radar data files available) was composited at 250 m resolution within 100 km of each radar (Figure 3). While nearly all of coastal Southern California has experienced NCFR activity over the past 26 years, their characteristics have been spatially variable. Multiple intense NCFRs appear to have impacted San Diego County, though it is difficult to discern whether the KNKX radar's low elevation favors stronger returns. The KVBX radar had considerably less data available for the NCFR record (noted in Section 2.2), and the KVTX and KSOX radars have a comparatively high base elevation scan (Figure 1), so it is unclear whether the apparent east-west gradient in reflectivity intensity is physical or an artifact of the observing network. The issues of beam blockage and radar height are also evident in Figure 3 as spatially discontinuous and apparently non-physical regions of weak maximum composite reflectivity (e.g., west of the Channel Islands and north of the Transverse Ranges), which further render the influence of topography on NCFR propagation challenging to discern.

3.2.3. Propagation

A subsample of 10 individual NCFRs were tracked through radar imagery to characterize their typical propagation. For each NCFR, 1-hr of 5-min reflectivity imagery (inclusive; 13 total individual volume scans) was used to identify and track the center of a single core region within the larger NCFR structure. The center of each tracked NCFR core was approximated as the median coordinates of all grid points within the core. Using the starting and ending center points over a single hour, the distance, azimuth angle, and speed of the core's propagation was calculated. Due to the simple tracking method employed, the 10 chosen NCFRs represent events where processed NEXRAD radar imagery of a single core region within each event was easily identifiable and uninterrupted for a 1-hr period. Any spatial or temporal characteristics between tracked events was not considered.

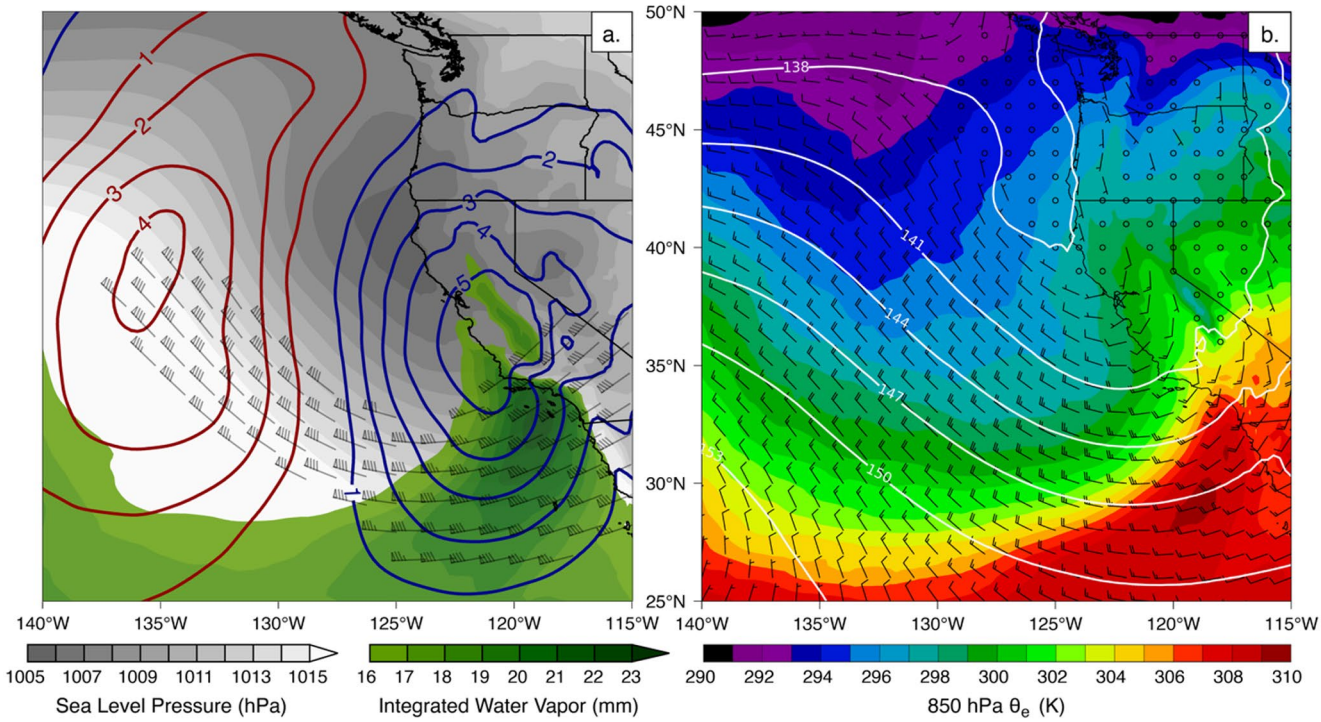

Figure 4. ERA5 mean SLP (gray shade; hPa), precipitable water (green fill; mm) and 250 hPa winds (barbs; kt for speeds >77.75 kts [40 m s^{-1}]) 6-hr prior to the peak of 76 NCFR episodes. The mean SLP change from 24 to 6-hr prior to peak NCFR strength in radar imagery (contours). Decreasing SLP tendency is shown in blue and increasing in red (a). 850 hPa θ_e (color fill; K), geopotential height (contour; dam), and winds (barbs; kt) 1-hr prior to peak NCFR strengh (b).

On average, single cores propagated a distance of 51 km in 1-hr (average speed of 14.2 m s^{-1}), with a range of 36–67 km (10–18.5 m s^{-1}). The average azimuth angle of propagation was 59° (ENE) with a range of 34–100° (NNE to ESE). These observations are similar to those reported for individual events by Cannon et al. (2018, 2020). The average maximum reflectivity value observed across events was 61 dBZ (range of 56–69 dBZ), while the average maximum 95th percentile reflectivity value was 55 dBZ (range of 52–61 dBZ). Note that NWS does not typically convert reflectivity >55 dBZ to precipitation rate as the sampled volume is assumed to contain ice. Although the sample size ($n = 10$) was small, the aforementioned propagation statistics (Table S1 in Supporting information S1) provide preliminary insight to the movement of NCFR cores within Southern California.

3.3. Synoptic Conditions Preceding NCFR Development

Though a variety of large-scale conditions support NCFR development, composites revealed common characteristics. The sea level pressure (SLP) composite mean of 76 NCFR episodes 6-hr prior to their peak reflectivity demonstrated a characteristic surface cyclone immediately offshore of northern California, centered at approximately 125°W, 40°N (Figure 4a). A composite integrated water vapor maximum was present over the Bight (Figure 4a). SLP tendency over the 18-hr period beginning 24-hr prior to the NCFR peak until the time of the mean SLP composite (6-hr prior to the peak) demonstrated a negative tendency of ~5 hPa over the 18-hr period (Figure 4a). The largest pressure falls occurred immediately west of the Bight, under the left exit region of a 250 hPa jet streak (Figure 4a). The surface pressure falls are characteristic of a system with ageostrophic frontal circulation in the region of enhanced deepening that would support frontogenesis, frontally-forced ascent, and NCFR development (e.g., Cannon et al., 2020). Composite 850 hPa derived equivalent potential temperature and winds 1-hr prior to NCFR peak showed an 8 K gradient and ~45° shift in wind direction (from westerly to south-southwesterly) across the Bight (Figure 4b), characteristic of a cold front. The composite signal is comprised of a range of cyclone intensities, including a handful of extreme events with considerably deeper cyclones and more rapid deepening (the type of synoptic conditions that have been investigated in impactful case studies; e.g., Cannon et al., 2018, 2020; Oakley, Cannon, Munroe, et al., 2018).

3.4. Hazards Associated With NCFRs

The record of NWS flash flood, severe thunderstorm, and tornado warnings was compared to the created NCFR catalog to highlight associated hazards, similar to an analysis performed by Cordeira et al. (2018) for atmospheric rivers. NWS-issued warnings are forecasts; their verification is conditional on the intersection of the forecasted meteorological phenomenon, such as a NCFR, and some physical point of concern (e.g., a flood prone watershed, or a recently burned area). Therefore, the issuance of a warning does not necessarily indicate the occurrence of impacts. However, the issuance of warnings lends insight to the relative importance of NCFRs to weather-related threats to life and property in the region.

The 76 NCFR episodes identified were associated with 279 flash flood warnings, 110 severe thunderstorm warnings, and 18 tornado warnings–these account for 28%, 43%, and 36%, respectively, of all warnings in those categories issued over the study period. In all, 31 events were associated with no warnings, 45 had at least one warning, and 15 had more than 10, indicating that a handful of NCFR episodes in recent decades were responsible for a disproportionately large number of NWS warnings (45 individual dates represent ∼1% of the study period but account for ∼32% of the warnings). Although the NCFR climatology features a set of extreme precipitation events driven by common meteorological processes (e.g., a deepening cyclone), the behavior of any individual NCFR, the intensity of its precipitation, and its regional impacts exist on a spectrum. Case studies have focused exclusively on the upper end of that spectrum, but future work to determine the lead time from identification to landfalling impacts, as well as the predictability of these events in operational numerical weather prediction systems, will benefit from analysis of the full record of event characteristics.

4. Summary and Discussion

The first known long-term record of NCFR occurrences in the Southern California Bight is presented here and used to describe NCFR climatological characteristics and impacts. On average, three NCFR events were observed in the Bight per year with as few as zero and as many as 11 in any given year. NCFRs were found to be most common in January, February, and March. On average, NCFRs cores move across the Bight at a speed of approximately 14.2 m s^{-1} in an east-northeastward direction. A composite of the synoptic conditions across 76 NCFR episodes in the climatology reveals a surface cyclone just offshore of Northern California (∼125°W, 40°N) and deepening sea level pressure over Central and Southern California in the 18-hr preceding the maximum NCFR intensity in the Bight. Roughly 60% of identified NCFR episodes resulted in the NWS issuing at least one flash flood, severe thunderstorm, or tornado warning.

The NCFR climatology was developed through manual methods, as automated radar detection methods that have been used for convective hazard applications in other regions were not suitable in Southern California due to both the meteorological conditions being sampled and limitations of the radar network. The potential for not identifying NCFR events does exist due to radar limitations and the subjective nature of the analyses, though the vast majority of events display spatially similar synoptic meteorology environments prior to peak strength (Figure S3 in Supporting information S1), and Monte Carlo random sampling of a subset of events indicate that the results are insensitive to the inclusion or exclusion of individual NCFRs. The work presented here suggests that NCFR detection with radar is important, and that the challenges encountered are illustrative of necessary considerations in employing radar data toward developing convective hazard climatologies in other regions with limited coverage. As progress continues toward rectifying radar and other related observational gaps (e.g., Ralph et al., 2014), and applications for the data become apparent, the steps taken to generate this NCFR climatology for Southern California will prove transferrable to other regions with complex terrain impacting radar coverage.

This comprehensive record of NCFRs is an important step toward improved observation and understanding of NCFR characteristics relative to the local area and climatology, overcoming forecasting challenges, and developing an objective identification algorithm. The catalog developed here can serve as a training dataset to develop an automated identification methodology, which could then be applied to other NCFR impacted locations, and can be used to evaluate the ability of numerical weather prediction models to resolve fine scale features in NCFRs that have been shown to be challenging to predict with accuracy (Cannon et al., 2020). Improved forecast skill and understanding of NCFR characteristics supports the protection of life and property in areas susceptible to impacts associated with short-duration, high intensity rainfall, such as urban and recent burn areas.

Data Availability Statement

The NCFR catalog and an associated README file is archived through the UC San Diego Library's Digital Collections website (de Orla-Barile et al., 2021, https://doi.org/10.6075/J06T0K5V). Level II NEXRAD reflectivity data was downloaded from NOAA's publicly-available archive on Amazon Web Services (https://registry.opendata.aws/noaa-nexrad/), and was processed and gridded for plotting using the Lidar Radar Open Software Environment (LROSE; Blaze Release; 2019; http://lrose.net/index.html). ERA5 data were acquired from the ECMWF Copernicus programme (Copernicus Climate Change Service, 2017). Neither the European Commission nor ECMWF is responsible for any use that may be made of the Copernicus Information or Data it contains.

Acknowledgments
Funding for this work was provided by the California Department of Water Resources Atmospheric River Program Phase II, grant 4600013361 and the National Oceanic and Atmospheric Administration (NOAA) Collaborative Science, Technology, and Applied Research (CSTAR) Program under grant NA19NWS4680004.

References

Bolton, D. (1980). The computation of equivalent potential temperature. *Monthly Weather Review*, *108*(7), 1046–1053. https://doi.org/10.1175/1520-0493(1980)108<1046:tcoept>2.0.co;2

Cannon, F., Hecht, C. W., Cordeira, J. M., & Ralph, F. M. (2018). Synoptic and mesoscale forcing of southern California extreme precipitation. *Journal of Geophysical Research: Atmospheres*, *123*(24), 13714–13730. https://doi.org/10.1029/2018JD029045

Cannon, F., Oakley, N. S., Hecht, C. W., Michaelis, A., Cordeira, J. M., Kawzenuk, B., et al. (2020). *Observations and predictability of a high-impact narrow cold-frontal rainband over Southern California on 2 February 2019* (pp. 1–40). Weather Forecasting.

Carbone, R. E. (1982). A severe frontal rainband. Part I. Stormwide hydrodynamic structure. *Journal of the Atmospheric Sciences*, *39*(2), 258–279. https://doi.org/10.1175/1520-0469(1982)039<0258:asfrpi>2.0.co;2

Clark, M. R. (2013). A provisional climatology of cool-season convective lines in the UK. *Atmospheric Research*, *123*, 180–196. https://doi.org/10.1016/j.atmosres.2012.09.018

Clark, M. R., & Parker, D. J. (2020). Synoptic-scale and mesoscale controls for tornadogenesis on cold fronts: A generalised measure of tornado risk and identification of synoptic types. *Quarterly Journal of the Royal Meteorological Society*, *146*(733), 4195–4225. https://doi.org/10.1002/qj.3898

Copernicus Climate Change Service (C3S). (2017). *ERA5: Fifth generation of ECMWF atmospheric reanalyses of the global climate. Copernicus climate change service climate data store (CDS)* (p. 2020). Retrieved from https://cds.climate.copernicus.eu/cdsapp#!/home

Cordeira, J. M., Neureuter, M. M., & Kelleher, L. D. (2018). Atmospheric rivers and national weather service watches, warnings, and advisories issued over California 2007–2016. *Journal of Operational Meteorology*, *6*(8), 87–94. https://doi.org/10.15191/nwajom.2018.0608

County of Santa Barbara. (2018) *Thomas fire and 1/9 debris flow recovery strategic plan*. Retrieved from http://www.countyofsb.org/asset.c/4359#:~:text=The%20purpose%20of%20the%20Thomas,and%20the%20resulting%201%2F9

Daly, C., Neilson, R. P., & Phillips, D. L. (1994). A statistical-topographic model for mapping climatological precipitation over mountainous terrain. *Journal of Applied Meteorology*, *33*(2), 140–158. https://doi.org/10.1175/1520-0450(1994)033<0140:astmfm>2.0.co;2

de Orla-Barile, M., Cannon, F., Oakley, N. S., & Ralph, F. M. (2021). *Southern California narrow cold-frontal rainband (NCFR) catalogue (1995–2020)*. UC San Diego Library Digital Collections. https://doi.org/10.6075/J06T0K5V

Doviak, R. J., & Zrnić, D. S. (1993). *Doppler radar and weather observations* (2nd ed., p. 562). Academic Press. https://doi.org/10.1016/C2009-0-22358-0

Gatzen, C. (2011). A 10-year climatology of cold-season narrow cold-frontal rainbands in Germany. *Atmospheric Research*, *100*(4), 366–370. https://doi.org/10.1016/j.atmosres.2010.09.018

Geerts, B., & Hobbs, P. V. (1995). A squall-like narrow cold-frontal rainband diagnosed by combined thermodynamic and cloud microphysical retrieval. *Atmospheric Research*, *39*(4), 287–311. https://doi.org/10.1016/0169-8095(95)00018-6

Haberlie, A. M., & Ashley, W. S. (2019). A radar-based climatology of mesoscale convective systems in the United States. *Journal of Climate*, *32*(5), 1591–1606. https://doi.org/10.1175/JCLI-D-18-0559.1

Hobbs, P. V., & Biswas, K. R. (1979). The cellular structure of narrow cold-frontal rainbands. *Quarterly Journal of the Royal Meteorological Society*, *105*(445), 723–727. https://doi.org/10.1002/qj.49710544516

Hobbs, P. V., Locatelli, J. D., Matejka, T. J., & Houze, R. A., Jr (1978). Air motions, mesoscale structure and cloud microphysics associated with a cold front. *Proceedings of the Conference on Cloud Physics and Atmospheric Electricity* (pp. 277–283). American Meteorological Society.

Houze, R. A., Hobbs, P. V., Biswas, K. R., & Davis, W. M. (1976). Mesoscale rainbands in extratropical cyclones. *Monthly Weather Review*, *104*(7), 8682–8878. https://doi.org/10.1175/1520-0493(1976)104<0868:mriec>2.0.co;2

James, P. K., & Browning, K. A. (1979). Mesoscale structure of line convection at surface cold fronts. *Quarterly Journal of the Royal Meteorological Society*, *105*(444), 371–382. https://doi.org/10.1002/qj.49710544404

Jorgensen, D. P., Pu, Z., Persson, P. O. G., & Tao, W.-K. (2003). Variations associated with cores and gaps of a Pacific narrow cold frontal rainband. *Monthly Weather Review*, *131*(11), 2705–2729. https://doi.org/10.1175/1520-0493(2003)131<2705:vawcag>2.0.co;2

Lamjiri, M. A., Dettinger, M. D., Ralph, F. M., Oakley, N. S., & Rutz, J. J. (2018). Hourly analyses of the large storms and atmospheric rivers that provide most of California's precipitation in only 10 to 100 hours per year. *San Francisco Estuary and Watershed Science*, *16*(4), 1–17. https://doi.org/10.15447/sfews.2018v16iss4art1

Lukashov, S. G., Lancaster, J. T., Oakley, N. S., & Swanson, B. J. (2019). Post-fire debris flows of 9 January 2018, Thomas Fire, southern California: Initiation areas, precipitation and impacts. *7th International Conference on Debris-Flow Hazards Mitigation*.

Maddox, R. A., Zhang, J., Gourley, J. J., & Howard, K. W. (2002). Weather radar coverage over the contiguous United States. *Weather and Forecasting*, *17*(4), 9272–9934. https://doi.org/10.1175/1520-0434(2002)017<0927:wrcotc>2.0.co;2

National Research Council. (2005). *Flash flood forecasting over complex terrain: With an assessment of the Sulphur Mountain NEXRAD in Southern California*. The National Academies Press. https://doi.org/10.17226/11128

Neiman, P. J., Martin Ralph, F., Persson, P. O. G., White, A. B., Jorgensen, D. P., & Kingsmill, D. E. (2004). Modification of fronts and precipitation by coastal blocking during an intense landfalling winter storm in southern California: Observations during CALJET. *Monthly Weather Review*, *132*(1), 242–273. https://doi.org/10.1175/1520-0493(2004)132<0242:mofapb>2.0.co;2

NOAA National Weather Service (NWS). (1991). *Radar operations center NOAA next generation radar (NEXRAD) level 2 base data*. (p. 2020). NOAA National Centers for Environmental Information. https://doi.org/10.7289/V5W9574V

Oakley, N. S., Cannon, F., Boldt, E., Dumas, J., & Ralph, F. M. (2018). Origins and variability of extreme precipitation in the Santa Ynez river basin of southern California. *Journal of Hydrology: Regional Studies*, *19*, 164–176. https://doi.org/10.1016/j.ejrh.2018.09.001

Oakley, N. S., Cannon, F., Munroe, R., Lancaster, J. T., Gomberg, D., & Ralph, F. M. (2018). Brief communication: Meteorological and climatological conditions associated with the 9 January 2018 post-fire debris flows in Montecito and Carpinteria, California, USA. *Natural Hazards and Earth System Sciences*, *18*(11), 3037–3043. https://doi.org/10.5194/nhess-18-3037-2018

Oakley, N. S., Lancaster, J. T., Hatchett, B. J., Stock, J., Ralph, F. M., Roj, S., & Lukashov, S. (2018). A 22-year climatology of cool season hourly precipitation thresholds conducive to shallow landslides in California. *Earth Interactions*, *22*(14), 1–35. https://doi.org/10.1175/EI-D-17-0029.1

Oakley, N. S., Lancaster, J. T., Kaplan, M. L., & Ralph, F. M. (2017). Synoptic conditions associated with cool season post-fire debris flows in the Transverse ranges of southern California. *Natural Hazards*, *88*(1), 327–354. https://doi.org/10.1007/s11069-017-2867-6

Parsons, D. B. (1992). An explanation for intense frontal updrafts and narrow cold-frontal rainbands. *Journal of the Atmospheric Sciences*, *49*(19), 1810–1825. https://doi.org/10.1175/1520-0469(1992)049<1810:aefifu>2.0.co;2

Prein, A. F., Liu, C., Ikeda, K., Bullock, R., Rasmussen, R. M., Holland, G. J., & Clark, M. (2017). Simulating North American mesoscale convective systems with a convection-permitting climate model. *Climate Dynamics*, *55*(1), 95–110. https://doi.org/10.1007/s00382-017-3993-2

Ralph, F. M., Dettinger, M., White, A., Reynolds, D., Cayan, D., Schneider, T., et al. (2014). A vision for future observations for western U.S. extreme precipitation and flooding. *Journal of Contemporary Water Research & Education*, *153*(1), 16–32. https://doi.org/10.1111/j.1936-704X.2014.03176.x

Rutz, J. J., Steenburgh, W. J., & Ralph, F. M. (2014). Climatological characteristics of atmospheric rivers and their inland penetration over the western United States. *Monthly Weather Review*, *142*, 905–921. https://doi.org/10.1175/MWR-D-13-00168.1

Sukup, S., Laber, J., Sweet, D., & Thomson, R. (2016). *Analysis of an intense narrow cold frontal rainband and the Springs Fire burn area debris flows of 12 December 2014*. NWS Technical Attachment 1601s. National Weather Forecast Office. Retrieved from https://www.weather.gov/media/wrh/online_publications/TAs/TA1601.pdf

Thompson, R. A. (2001). *Flash flood event of 6 February 1998: A case study*. (NWS Western Region Technical Attachment 01-08. National Weather Forecast Office. Retrieved from https://weather.gov/media/wrh/online_publications/TAs/ta0108.pdf

Trapp, R. J., Tessendorf, S. A., Godfrey, E. S., & Brooks, H. E. (2005). Tornadoes from squall lines and bow echoes. Part I: Climatological distribution. *Weather and Forecasting*, *20*(1), 23–34. https://doi.org/10.1175/WAF-835.1

Zacharaissen, J., Zeller, K., Nikolov, N., & McClelland, T. (2003). *A review of the forest service remote automated weather station (RAWS) network*. (USDA General Technical Report RMRS-GTR-119). U.S. Department of Agriculture, Forest Service, Rocky Mountain Research Station. https://doi.org/10.2737/RMRS-GTR-119